Nat. Hazards Earth Syst. Sci. Discuss., 2, 7119–7147, 2014
www.nat-hazards-earth-syst-sci-discuss.net/2/7119/2014/
doi:10.5194/nhessd-2-7119-2014

Natural Hazards and Earth System Sciences
Open Access
Discussions

A feasibility study on the influence of the geomorphological feature in identifying the potential landslide hazard

M. H. Baek[1] **and T. H. Kim**[2]

[1]Department of Fire and Disaster Prevention, Kangwon National University, Joongang-ro, Samcheok-si, Gangwon-do 245–711, Republic of Korea
[2]National Disaster Management Institute, Ministry of Safety and Public Administration, 136, Mapo-daero, Mapo-gu, Seoul 121–719, Republic of Korea

Received: 2 September 2014 – Accepted: 22 October 2014 – Published: 20 November 2014

Correspondence to: T. H. Kim (taihoon@ualberta.ca)

Published by Copernicus Publications on behalf of the European Geosciences Union.

Abstract

In this study we focused on identifying geomorphological features that control the location of landslides. The representation of these features is based on a high resolution DEM (Digital Elevation Model) derived from airborne laser altimetry (LiDAR) and evaluated by statistical analysis of axial orientation data. The main principle of this analysis is generating eigenvalues from axial orientation data and comparing them. The Planarity, a ratio of eigenvalues, would tell the degree of roughness on ground surface based on their ratios. Results are compared to the recent landslide case in Korea in order to evaluate the feasibility of the proposed methodology in identifying the potential landslide hazard. The preliminary landslide assessment based on the Planarity analysis well discriminates features between stable and unstable domain in the study area especially in the landslide initiation zones. Results also show it is beneficial to build the preliminary landslide hazard especially inventory mapping where none of information on historical records of landslides is existed. By combining other physical procedures such as geotechnical monitoring, the landslide hazard assessment using geomorphological features will promise a better understanding of landslides and their mechanisms, and provide an enhanced methodology to evaluate their hazards and appropriate actions.

1 Introduction

Landslides, reflecting the geomorphological process of the natural landscape, become a threat only when they interfere with our societies (Pestrong, 1976). They annually cause losses of many lives and have enormous economic impacts. There is a considerable attention about landslides since they usually make significant casualties and property damages (Aleotti and Chowdhury, 1999). Increasing costs are closely related to the expansion of population and development which result in residential areas near slopes. Through urban expansions, cities transform their surrounding environments

NHESSD
2, 7119–7147, 2014

and produce new risks (UNDP, 2004). Constructing residences, industrial structures, transportation, and lifelines around the slopes may decrease their stability. Therefore, landslides became disastrous events and, in turn, disturb and affect the well being of society. In developing countries, these impacts are even more severe (Schuster and Highland, 2007).

Once landslides occur, they usually leave features such as scarps, cracks, and displaced materials on the ground. Identifying these geomorphological features in order to determine the potential landslide area based on historical evidences would provide valuable information in assessing the landslide hazard. Recent distinct characteristic in this field is utilizing recent remote sensing technologies. For example, Kimura and Yamaguchi (2000) used a synthetic aperture radar interferometry (InSAR) with precipitation data for modeling landslide movements in northern Japan. They noted that the model powered by InSAR technology can account for the complex landslide movements showing either shallow or deep seated landslide behaviours when ground surface measurements observed at the same location are difficult to recognize the overall movement mechanisms. Catani et al. (2005) also discussed the capability of the SAR interferometry technique for quantifying landform attributes. While InSAR technologies are focused on the recognition of dynamic behaviours of geomorphological landslide controlled features on ground surfaces in order to identify landslide movement mechanisms, the static quantification of landslide control attributes are carried out by a high resolution topographic information, which is obtained from LiDAR (Light Detection and Ranging) technique (Glenn et al., 2006). LiDAR can generate high resolution models which differentiate distinct landslide features such as steep scarps at the top, fan shaped lobes at the toe, and an irregular hummocky topography between top and bottom. These features can be evaluated based on their evolution by natural processes over time. The landslide inventory mapping enhanced by the LiDAR derived digital elevation model (DEM) can provide not only the exact boundary of previous landslides but also an insight on the internal deformation of the landslide body (McKean and Roering, 2004). However, approaches to find these remnants of landslides have several limita-

NHESSD
2, 7119–7147, 2014

tions (Kim et al., 2012). Major issues are insufficient compilation of key features and changes of topography by other processes such as weathering. Implementing landslide hazard assessments with incomplete information would lead to erroneous decisions about ongoing and future developments of landslides (Kim, 2012).

In this study, therefore, we focused on identifying geomorphological landslide controlled features in order to overcome several limitations as discussed before. Representation of these is based on a high resolution DEM derived from airborne laser altimetry (LiDAR) and evaluated by statistical analysis of axial orientation data. Results are compared to the recent landslide whether the proposed methodology assures the potential landslide hazard or not.

2 Methodology

Analyzing a terrain, whether rough or smooth, is an important part for landslide studies, in which understanding a terrain is essential for future development of landslides. Finding geomorphological features which are generated by landslides is the main purpose of the landslide inventory mapping that gathers information from various sources such as aerial photographs and archives. However, the limited time span and evolution of topography by natural processes may have restricted any meaningful progress using terrain features. Various approaches were examined to overcome these limitations (Glenn et al., 2006; Kaplan, 2006; Delacourt et al., 2007; Sappington et al., 2007; Schulz, 2007; van Den Eeckhaut et al., 2007; Teza et al., 2008; Grohmann et al., 2009).

One promising methodology describing geomorphological landslide controlled features is the statistical analysis of axial orientation data in a three dimensional space. Obtained from the orientation tensor, they are useful to analyze the randomness in three dimensional directional data (Woodcock, 1977; Woodcock and Naylor, 1983).

Based on the spherical distribution of directional and non-directional data it is shown that typical characteristics of spherical distribution are equivalent to the determination of eigenvalues and eigenvectors especially of a symmetric three by three matrix which

NHESSD
2, 7119–7147, 2014

comprises direction cosines (Watson, 1966). Consider N points of the unit mass of (l_i, m_i, n_i), where $N = 1, 2, \ldots, N$ and suppose that $\boldsymbol{u}$ is a true or preferred direction through the centre of the sphere, the moment of inertia I of the set of N points of unit observation data about $\boldsymbol{u}$ can be described as follows (Watson, 1966):

$$I = N - \boldsymbol{u}'\mathbf{M}\boldsymbol{u} = N - \sum_{j=1}^{3}\sum_{k=1}^{3} u_j M_{jk} u_k \quad (1)$$

where $\mathbf{M}$ is an orientation matrix, a three by three matrix consisting sums of the cross products of direction cosines of the unit mass, (l_i, m_i, n_i). It is given by:

$$\mathbf{M} = \begin{pmatrix} \sum l_i^2 & \sum l_i m_i & \sum l_i n_i \\ \sum m_i l_i & \sum m_i^2 & \sum m_i n_i \\ \sum n_i l_i & \sum n_i m_i & \sum n_i^2 \end{pmatrix} \quad (2)$$

The eigenvalues of the orientation matrix are calculated from roots of the characteristic equation. Therefore:

$$\det(\mathbf{M} - \lambda\mathbf{I}) = 0 \quad (3)$$

where det is the determinant of $\mathbf{M}$, $\mathbf{I}$ is the identity matrix. Roots of the characteristic equation are the eigenvalues, λ_i $(i = 1, 2, 3;\ \lambda_1 > \lambda_2 > \lambda_3)$, and corresponding vectors are the eigenvectors, $\boldsymbol{v}_i$ $(i = 1, 2, 3)$. Three eigenvalues are always positive and add to N while three eigenvectors are always perpendicular to each other (Watson, 1966). A normalized form of the eigenvalues can be obtained from dividing by the number of unit observation points, N:

$$S_j = \frac{\lambda_j}{N}, \quad j = 1, 2, 3 \quad (4)$$

The determination of the typical distribution of eigenvalues and eigenvectors are dependent of the spherical location of the axial orientation data. Watson (1966) proposed

NHESSD
2, 7119–7147, 2014

two distinct distributions on a spherical surface: (a) a clustered distribution and, (b) a girdle distribution, which are represented by the different magnitude and direction of eigenvalues and eigenvectors (Fig. 1). If the unit mass are clustered at both ends of the great circle in a sphere (Fig. 1a), indicating either uni or bimodal distributions, the moment of inertia in Eg. (1) along this axis would be small and therefore, large eigenvalue and eigenvector are induced from the small value of the moment of inertia. Two other small values of eigenvalue and eigenvector are comparable and located along the diameter of the great circle. Obviously fairly equal eigenvalues would represent no preferred direction which having the uniform distribution in observation data. For the clustered distribution, therefore, one large eigenvalue and other two small eigenvalues are usually observed.

On the other hand, a girdle distribution, where the unit mass are positioned around the great circle (Fig. 1b) would require the greatest moment of inertia which leads to a minimum eigenvalue at the axis perpendicular to the great circle. Other two moments of inertia along the diameter of the great circle have the least values and they cause large eigenvalues and eigenvectors both of which have similar values. The girdle distribution, therefore, is generally indicated by one small eigenvalue with two large eigenvalues. Detailed types of the spherical distributions based on eigenvalues and eigenvectors of the orientation matrix **M** are summarized in Table 1.

The principle of the statistical analysis proposed by this study is generating eigenvalues that represent typical values for the degree of roughness. For more clear identification, we introduce one non-dimensional parameter, composing the ratio of eigenvalues (Woodcock, 1977; Woodcock and Naylor, 1983):

$$\text{Planarity} = \ln\left(\frac{S_1}{S_2}\right) \tag{5}$$

The Planarity (P), the natural logarithmic proportion of the eigenvalue S_1 relative to S_2, can be a good indicator in describing the level of roughness on ground surface (Kim et al., 2012). The evaluation of the Planarity is especially beneficial when large amounts

NHESSD
2, 7119–7147, 2014

of field data are acquired and compared, which contain the directional characteristic of materials.

The procedure to identify geomorphological features for landslides is performed as follows. First, the DEM of 1 by 1 m spatial resolution is used for the calculation. It is taken from 2009 LiDAR dataset. Direction cosines are then calculated from the slope and aspect values. Each element of the orientation matrix shown in Eq. (2) is then represented by these direction cosines.

All cell-based (i.e., raster based) calculations such as summation of elements in the orientation matrix by the moving window (3 by 3) and their geographical representations augmented by the Spatial Analyst tool embedded in ArcGIS®. A cubic equation is employed to determine three eigenvalues. These are then normalized by N total cells. Finally, Planarity (P) is introduced by a ratio of eigenvalues. Thresholds of each Planarity are based on appropriate representation of characteristics of different units consisting the study area such as major valleys, secondary tributaries, gently rolling surfaces, and smooth surfaces. High planarity may indicate a smooth ground surface that has a preferred direction while low one may have a less preferred direction, describing a rough ground surface, and after all, may reflect previous landslides containing related features such as scarps, cracks, and displaced materials (McKean and Roering, 2004; Kasai et al., 2009).

3 Overview of the study area

Mt. Umyeon, located in the south of Seoul Metropolitan City, Republic of Korea, is a part of major mountains traversing the southern part of Seoul in the direction of north-northeast (Fig. 2). It is consisted by relatively lower hilly mountains, which is based on a variety of gneisses by tectonic movements and weathering processes (Song et al., 2011). Major geological characteristic in the study area is dominated by the Biotite Banded Gneiss and Augen Gneiss, Granitic Gneiss, Leuco-cratic Gneiss, and Fine-grained Gneiss take small parts (Hong and Lee, 1982). Due to characteristics of

NHESSD
2, 7119–7147, 2014

gneisses such as severe weathering and multiple faults, and geomorphological defects such as many trails and military bases, the study area would have a high susceptibility to landslides. Figure 3 described distinct geological aspects of the study area.

The 2011 landslide disasters in the study area were initiated on 27 July 2011. Major landslide areas, which indicated in Fig. 2, are: (a) Ramian and Sindonga APTs. (Site A), (b) Jeonwon-maul (Site B), (c) Hyungchon-maul (Site C). Table 2 summarizes general information on these sites and detailed descriptions of individual landslide are given in the following sections.

3.1 Site A (Ramian and Sindonga APTs)

Site A is located in the north of Mt. Umyeon and was affected by two landslides in different time span. The first landslide initiated at 8.40 a.m. and second one occurred at 10.00 a.m. on 27 July 2011. Both started their movement around roof areas of the mountain and flowed rapidly along the previous drainage channels. Displaced material overflew the road and hit the residential areas opposite to Mt. Umyeon (Fig. 4). These resulted five casualties in total. Fast movement of displaced materials and existence of previous channels made us to classify those landslides as debris flow (Hungr et al., 2014).

3.2 Site B (Hyungchon-maul)

Site B sat on the south east of Mt. Umyeon and have a major gully and eight small tributaries over the area. Total 30 landslides started their movements on 27 July 2011, flooded most residences within the site, and finally made one casualty (Fig. 5). There was a reservoir located on the middle of the mountain and failed by overflowing of water due to heavy rainfall intensity of over 85.5 $mm\,h^{-1}$. As similar to other sites, the types of landslides are debris flows progressing along a major gully with a help of other small tributaries. Thick colluviums deposits, average of 1 m, were often found in this

NHESSD
2, 7119–7147, 2014

area and up to 5 m of these were located where gullies are merged each other (Song et al., 2011).

3.3 Site C (Jeonwon-maul)

Located in the west of Mt. Umyeon, landslides in Site C initiated in the morning of 27 July 2011 and resulted six casualties (Fig. 6). Landslides were classified as debris flows because of their typical characteristics such as a fast downward movement of displaced materials along the existing gullies. Numbers of landslides in this site were reported as 22 and their average slope angles at initiation and transition zones of landslides were 27 and 15.6°, respectively. These are closely related to what VanDine (1996) described on debris flow with typical slope angles of greater than 25 and 15° for each individual zone. Average length of transition zone was recorded as 454.4 m (Yoo et al., 2014).

The main cause of the landslides in the study area, even though the main causal factor of this disastrous event is still unclear, was precipitation, which classifies into two different domains based on the temporal variation: (a) antecedent rainfall, (b) daily rainfall. Firstly, an antecedent rainfall of 463.0 mm fell within two weeks before the landslide events were occurred. This made the ground surface fully or almost fully saturated. Secondly, a heavy daily rainfall amounting 342.5 mm fell into the study area. It took about 74 % of antecedent rainfall. The rainfall intensity of the first impacted landslide areas was 68.5 mm h^{-1} (Fig. 7). Based on the rainfall records, the landslides in the study area may be initiated by the high intensity daily rainfall with the help of the saturated condition of the ground surface by long-term antecedent rainfall.

4 Results and discussion

In this study we employed a statistical analysis using axial orientation data in order to identify the geomorphological features of landslides. The main principle of this analysis

NHESSD
2, 7119–7147, 2014

is generating eigenvalues from axial orientation data and comparing their values. The Planarity (P) would tell the degree of roughness on ground surface based on their ratios. The extent of the area for analysis is defined by LiDAR dataset acquired in 2009 before landslides occurred. The topographic overview of the study area is shown in Fig. 2.

Figure 8 shows the spatial distribution obtained from the Planarity over the study area. The distribution is limited to steep slope areas more than 15° in slope values and Planarity beyond the extent is ignored since it could not describe a natural topography but an anthropogenic effect on ground profile. Figure 9 indicates representative values of Planarity occupying the effective study area.

Based on the Planarity analysis shown in Figs. 8 and 9, the lowest Planarity (less than three), defined by this study as "Very rough" areas, can be found in major valleys, secondary tributaries, and upper mountain areas near the army base and take 0.9 % of the total evaluated area. Results also indicate the "Moderately rough (Planarity is less than five)" areas would cover 14.3 % of the effective study area and these are usually wrapping the very rough areas. On the other hand, "Relatively flat" areas, the Planarity is less than seven, can be found in most gentle slopes. Majorities (about 50.6 %) of the evaluated area are included in this category. High Planarity of less than nine usually covers the other parts of gentle slopes. These areas, "Mostly flat", take 28.4 % of the evaluated study area. Finally, the "Completely flat" areas, over the value of nine, are concentrated on the few anthropogenic places where constructed within or boundary of the mountain and usually combined with "Mostly flat" areas (5.7 % of the evaluated study area).

In order to show the benefit of the Planarity analysis in preliminary landslide hazards, the mean slope value is employed since ignoring gentle slope areas in the analysis would give clear understanding of landslide hazards in the study area. Kim et al. (2012) noted that combining the Planarity with slope values can improve a capability of the landslide hazard assessment. Figure 10 illustrates the Planarity where the individual cell has over the mean slope value of 19°.

NHESSD
2, 7119–7147, 2014

And finally, the modified Planarity is implemented to representative landslide areas in 2011, i.e., Sites A to C for evaluating its suitability as a preliminary landslide hazard assessment. Figures 11 to 13 show the typical landslide characteristics observed in each site.

Figure 11a shows the aerial photo in Site A, which is obtained before the landslide. There was a landslide that was in the relict state and might be generated prior to 2011. The upstream part covered by forests would give a clue of the temporal variation since the landslide has occurred. The modified Planarity was draped on this area (Fig. 11b). Very rough areas are located in upper mountain areas where we believed those are scarps and the landslide might be initiated from these zones. The other can be found along the valley bottom. The actual landslide in 2011 clearly showed that landslides initiated adjacent very rough areas determined by Planarity (Fig. 11c). This consistency can also be found in Sites B and C (Figs. 12 and 13).

Even though there are various limitations which might come from the visual observation, the proposed methodology, the Planarity analysis, can provide a useful framework to understand the initial state of landslides without any other conventional approach. It also provides a fundamental data for the landslide inventory mapping, which is the initial form of the landslide hazard assessment. Combined with other physical consideration such as geotechnical monitoring for ongoing landslide movements, its feasibility as an indicator of the landslide hazard assessment can be enhanced and also suggests appropriate mitigation measures.

5 Conclusions

In this study we have delineated geomorphological features of recent landslides observed in the recent landslide area. The usefulness of them in utilizing for the preliminary landslide hazard also discussed. The Planarity, based on the statistical analysis of axial orientation data, provides benefits when landslide controlled features are identified by high resolution spatial data such as a LiDAR generated DEM.

NHESSD
2, 7119–7147, 2014

The preliminary landslide assessment using the Planarity well discriminates features between stable and unstable domain in the study area especially in the landslide initiation zones. Based on the study area the Planarity has various portions of occupied areas from less than one to 51 % and these roughly represent characteristics of different units consisting slopes such as major valleys, secondary tributaries, gently rolling surfaces, and smooth surfaces. The three specific cases in the study areas also indicate that areas designated as "Very rough" category where the potential landslide hazard is relatively high are closely related to the actual landslide initiation zones.

Results are also useful in the landslide inventory mapping without information on historical records of landslides. By combining other physical procedures, the landslide hazard assessment proposed in this study will promise a better understanding of landslides and their mechanisms, and provide an enhanced methodology to evaluate their hazards and appropriate actions.

References

Aleotti, P. and Chowdhury, R.: Landslide hazard assessment: summary review and new perspectives, B. Eng. Geol. Environ., 58, 21–44, 1999. 7120

Catani, F., Farina, P., Moretti, S., Nico, G., and Strozzi, T.: On the application of SAR interferometry to geomorphological studies: estimation of landform attributes and mass movements, Geomorphology, 66, 119–131, 2005. 7121

Delacourt, C., Allemand, P., Berthier, E., Raucoules, D., Casson, B., Grandjean, P., Pambrun, C., and Varel, E.: Remote-sensing techniques for analysing landslide kinematics: a review, B. Soc. Geol. Fr., 178, 89–100, 2007. 7122

Glenn, N. F., Streutker, D. R., Chadwick, D. J., Thackray, G. D., and Dorsch, S. J.: Analysis of LiDAR-derived topographic information for characterizing and differentiating landslide morphology and activity, Geomorphology, 73, 131–148, 2006. 7121, 7122

Grohmann, C. H., Smith, M. J., and Riccomini, C.: Surface roughness of topography: a multiscale analysis of landform elements in Midland Valley, Scotland, in: Proceedings of Geomorphometry, 31 August–2 September 2009, Zurich, Switzerland, 140–148, 2009. 7122

NHESSD
2, 7119–7147, 2014

Hong, S. H. and Lee, B. J.: Geological Map of Korea – Map and Explanatory Description of Dungeon Sheet, Korean Institute of Geoscience and Mineral Resources, Daejeon, Korea, 1–19, 1982. 7125, 7137
Hungr, O., Leroueil, S., and Picarelli, L.: The Varnes classification of landslide types, an update, Landslides, 1, 167–194, 2014. 7126
Kaplan, V.: Using textural information for classification of remote sensing imagery, in: Proceedings of the International Symposium GIS Ostrava 2006, Ostrava, Czech Republic, 23–25 January 2006, available at: http://gis.vsb.cz/GISEngl/Conferences/GIS_Ova/GIS_Ova_2006/Proceedings/Referaty/kaplan.html (last access: 20 November 2014), 2006. 7122
Kasai, M., Ikeda, M., Asahina, T., and Fujisawa, K.: LiDAR-derived DEM evaluation of deep-seated landslides in a steep and rocky region of Japan, Geomorphology, 113, 57–69, 2009. 7125
Kim, N. J. and Hong, S. H.: Geological Map of Korea – Map and Explanatory Description of Anyang Sheet, Korean Institute of Geoscience and Mineral Resources, Daejeon, Korea, 1–20, 1975. 7137
Kim, T. H.: Landslide hazard assessment, Town of Peace River, Alberta, Ph.D. thesis, Department of Civil and Envrionmental Engineering, University of Alberta, Edmonton, 2012. 7122
Kim, T. H., Cruden, D. M., and Martin, C. D.: Identification of geomorphological features of landslides using airborne laser altimetry, in: Proceedings of the 11th International Symposium on Landslides and 2nd North American Symposium on Landslides, 3–8 June 2012, Banff, Alberta, 567–573, 2012. 7122, 7124, 7128
Kimura, H. and Yamaguchi, Y.: Detection of landslide areas using satellite radar interferometry, Photogramm. Eng. Remote Sens., 66, 337–344, 2000. 7121
Mardia, K. V.: Statistics of Directional Data, Academic Press, London, 1972. 7133
McKean, J. and Roering, J.: Objective landslide detection and surface morphology mapping using high-resolution airborne laser altimetry, Geomorphology, 57, 331–351, 2004. 7121, 7125
Pestrong, R.: Landslides – the descent of man, California Geol., 29, 147–151, 1976. 7120
Sappington, J. M., Longshore, K. M., and Thompson, D. B.: Quantifying landscape ruggedness for animal habitat analysis: a case study using bighorn sheep in the Mojave Desert, J. Wildlife Manage., 71, 1419–1426, 2007. 7122
Schulz, W. H.: Landslide susceptibility revealed by LIDAR imagery and historical records, Seattle, Washington, Eng. Geol., 89, 67–87, 2007. 7122

NHESSD
2, 7119–7147, 2014

Schuster, R. L. and Highland, L. M.: Urban landslides: socioeconomic impacts and overview of mitigative strategies, the third Hans Cloos lecture, B. Eng. Geol. Environ., 66, 1–27, 2007. 7121

Song, Y. S., Jang, S. C., Chae, B. G., Hwang, Y. C., Ahn, J. H., Yoo, B. O., and Kwon, O. I.: Investigation on cause and establishment of mitigation for Mt. Umyeon Landlsides – final report, Seoul Metropolitan Government, Seoul, Korea, 262 pp., 2011. 7125, 7127

Teza, G., Pesci, A., Genevois, R., and Galaro, A.: Characterization of landslide ground surface kinematics from terrestrial laser scanning and strain field computation, Geomorphology, 97, 424–437, 2008. 7122

UNDP: Reducing disaster risk: a challenge for development, United Nations Development Programme, Bureau for Crisis Prevention and Recovery, One United Nations Plaza, New York, NY 10017, USA, 2004. 7121

van Den Eeckhaut, M., Poesen, J., Verstraeten, G., Vanacker, V., Nyssen, J., Moeyersons, J., van Beek, L. P. H., and Vandekerckhove, L.: Use of LIDAR-derived images for mapping old landslides under forest, Earth Surf. Proc. Land., 32, 754–769, 2007. 7122

VanDine, D. F.: Debris flow control structures for forest engineering, B. C. Ministry of Forest, Victoria, British Columbia, 68 pp., 1996. 7127, 7138

Watson, G. S.: The statistics of orientation data, J. Geol., 74, 786–797, 1966. 7123

Woodcock, N. H.: Specification of fabric shapes using an eigenvalue method, Geol. Soc. Am. Bull., 88, 1231–1236, 1977. 7122, 7124

Woodcock, N. H. and Naylor, M. A.: Randomness testing in three-dimensional rrientation data, J. Struct. Geol., 5, 539–548, 1983. 7122, 7124

Yoo, K. Y., Won, J. S., and Yoo, Y. M.: Additional and complementary research on landslide causes in Mt. Umyeon – final report, 452 pp., 2014. 7127, 7134

NHESSD

2, 7119–7147, 2014

Table 1. Detailed types of the spherical distributions based on eigenvalues and eigenvectors of the orientation matrix **M**. The order of eigenvalues is $\lambda_1 > \lambda_2 > \lambda_3$. R is the length of the resultant vector. Modified from Mardia (1972).

Eigenvalue distribution		Spherical distribution	Eigenvector distribution
$\lambda_1 \simeq \lambda_2 \simeq \lambda_3$		Random	No preferred orientation
$\lambda_1 > \lambda_2, \lambda_3$	$\lambda_2 \neq \lambda_3$	Unimodal if R is large	Concentrated at one end of $\boldsymbol{v}_1$
		Bimodal otherwise	Concentrated at both ends of $\boldsymbol{v}_1$
	$\lambda_2 \simeq \lambda_3$	Unipolar if R is large Bipolar otherwise	Rotational symmetry about $\boldsymbol{v}_1$
$\lambda_1, \lambda_2 > \lambda_3$	$\lambda_1 \neq \lambda_2$	Girdle	Girdle plane containing $\boldsymbol{v}_1$ and $\boldsymbol{v}_2$
	$\lambda_1 \simeq \lambda_2$	Symmetric girdle	Rotational symmetry about $\boldsymbol{v}_3$

NHESSD
2, 7119–7147, 2014

Table 2. Major landslides occurred in Mt. Umyeon, 2011. Each landslide area denoted by capital alphabet is also described in Fig. 2. Data are modified from Yoo et al. (2014). Cases being considered in this study area are indicated in the representative area name.

ID	Representative area name	No. of initiation zone
A	Ramian, Imgwang A.P.T.s (Site A)	6
B	Sindonga A.P.T. (Site A)	3
C	Hyungchon-maul (Site B)	30
D	Jeonwon-maul (Site C)	22
E	Bodeok-sa	14
F	Songdong-maul	18
G	Umyeonsan Tunnel	2
H	Educational Broadcasting System buildings	3
I	Gwanmun-sa	5
J	Gangnam Church	11
K	Seoul Arts Center	15
L	Deokwoo-am	5
M	Dwit-gol	16
	Total	150

NHESSD
2, 7119–7147, 2014

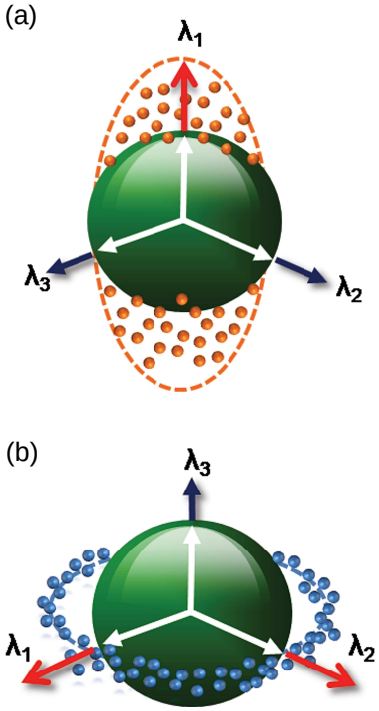

Figure 1. Distribution of axial orientation data on a spherical surface. **(a)** A clustered distribution. **(b)** A girdle distribution. In a clustered distribution, the axial orientation data have one large eigenvalue (λ_1) and two small eigenvalues (λ_2, λ_3). In contrast to this, the axial orientation data have one small eigenvalue (λ_3) and two large eigenvalues (λ_1, λ_2) in a girdle distribution.

NHESSD
2, 7119–7147, 2014

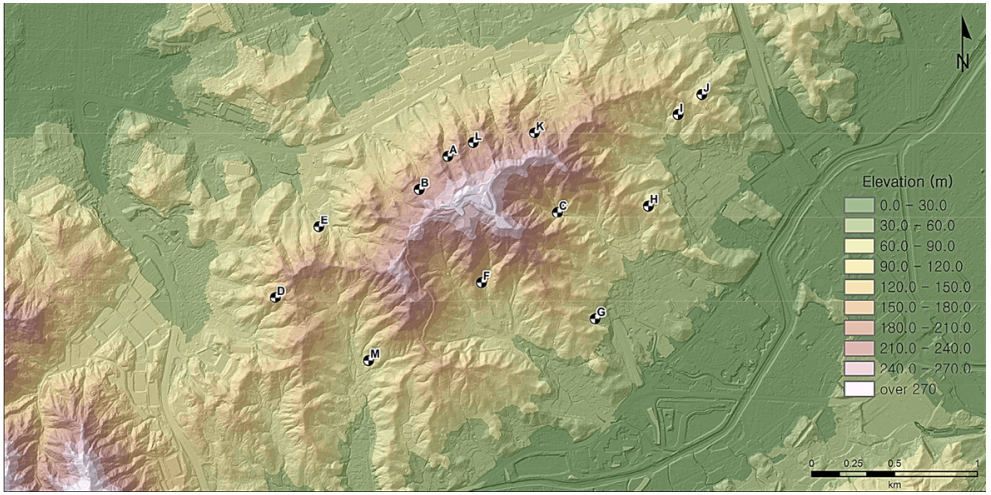

Figure 2. Location of the study area. Major landslide areas are also indicated. The position of each landslide is calculated as a mean centre for the individual landslide area: **(a)** Raminan A.P.T.; **(b)** Sindonga A.P.T.; **(c)** Hyunchon-maul; **(d)** Jeonwon-maul; **(e)** Bodeok-sa; **(f)** Songdong-maul; **(g)** Umyeonsan Tunnel; **(h)** Educational Broadcasting System buildings; **(i)** Gwanmun-sa; **(j)** Gangnam Church; **(k)** Seoul Arts Centre; **(l)** Deokwoo-am; and **(m)** Dwit-gol. The geographic coordinates of the landslide area A are 37.474013 (latitude) and 127.006552 (longitude) in decimal degrees.

NHESSD
2, 7119–7147, 2014

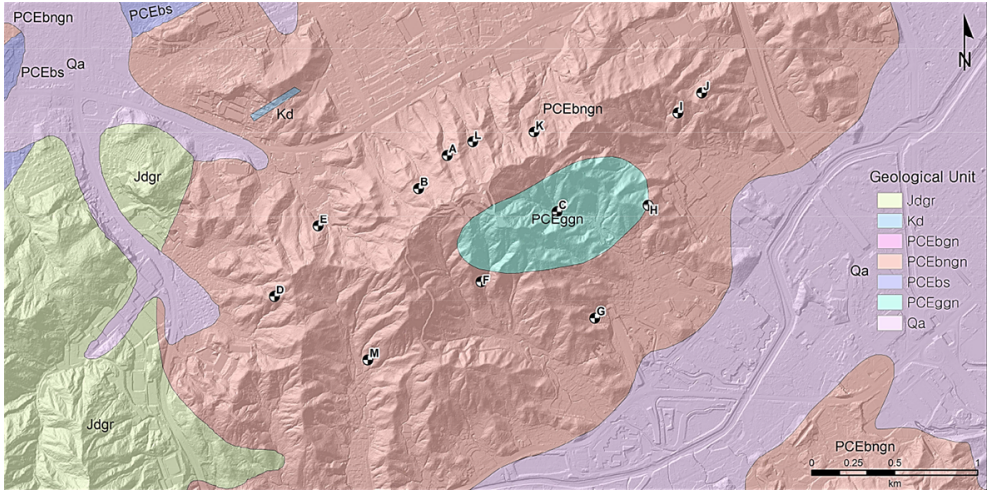

Figure 3. Geological map of the study area. Major landslide areas described in Fig. 2 are also shown. Representative geological units are: Jdgr (Jurassic daebo granite); Kd (dikes); PCEbngn (Pre-Cambrian Era banded biotite gneiss); PCEbs (Pre-Cambrian Era biotite schist); PCEggn (Pre-Cambrian Era granitic gneiss); and Qa (Quaternary alluvium). All geological information are based on Kim and Hong (1975) and Hong and Lee (1982).

NHESSD
2, 7119–7147, 2014

Influence of the geomorphological feature for the potential landslide hazard

M. H. Baek and T. H. Kim

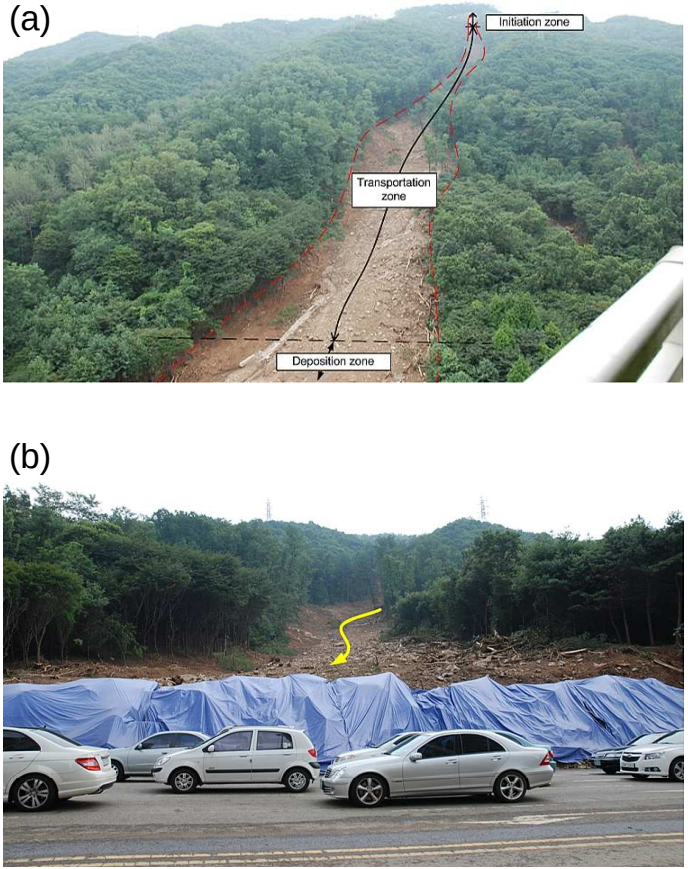

Figure 4. Landslides in Site A. **(a)** Overall trace of the landslide at Ramian A.P.T. Components of debris flows which VanDine (1996) proposed are described in the figure. **(b)** Bottom of the landslide at Singdonga A.P.T. where displaced materials traversed roads. The approximate direction of displaced materials is indicated by a yellow arrow.

NHESSD
2, 7119–7147, 2014

Figure 5. Landslides in Site B. **(a)** Impacted area by debris flows. **(b)** Upstream valley where debris flows were traced. The approximate direction of displaced materials is indicated by a yellow arrow, respectively.

NHESSD
2, 7119–7147, 2014

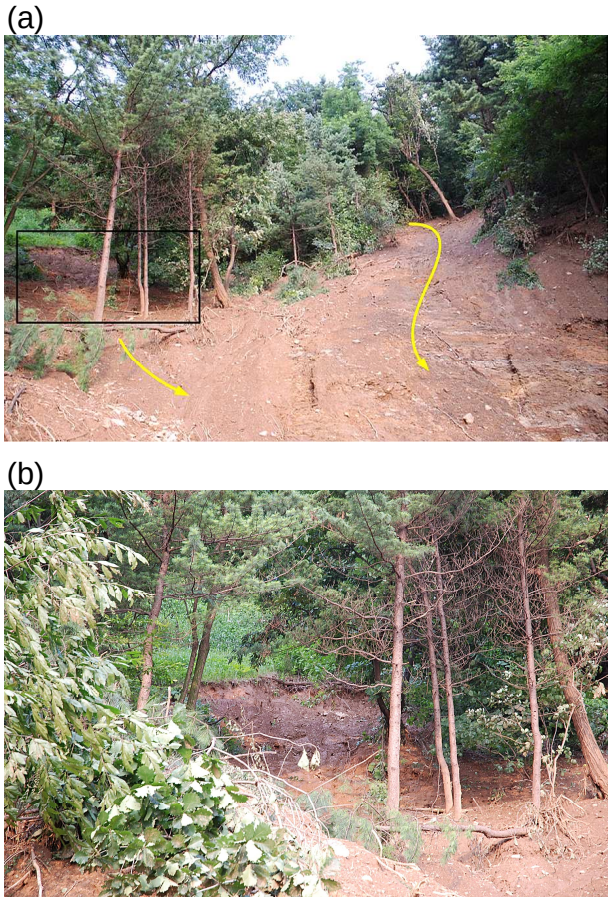

Figure 6. Landslides in Site C. **(a)** Initiation zone of debris flows. An area outlined by a black solid line indicates a closer look of one of the initiation zones in slopes **(b)**. The approximate direction of displaced materials is indicated by yellow arrows. **(b)** Close view of the initiation zone in slopes presented in **(a)**.

NHESSD
2, 7119–7147, 2014

Influence of the geomorphological feature for the potential landslide hazard

M. H. Baek and T. H. Kim

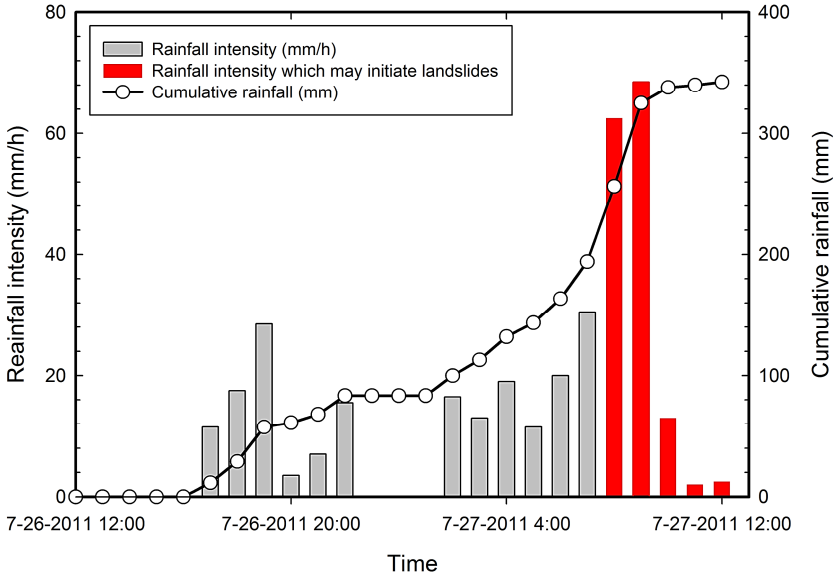

Figure 7. Temporal variation of the precipitation from 26 to 27 July 2011. Vertical bars indicate the rainfall intensity and cumulative rainfall is shown by a single line with circles. Some vertical bars in red represent the rainfall intensity which might cause landslides in the study area.

NHESSD
2, 7119–7147, 2014

Influence of the geomorphological feature for the potential landslide hazard

M. H. Baek and T. H. Kim

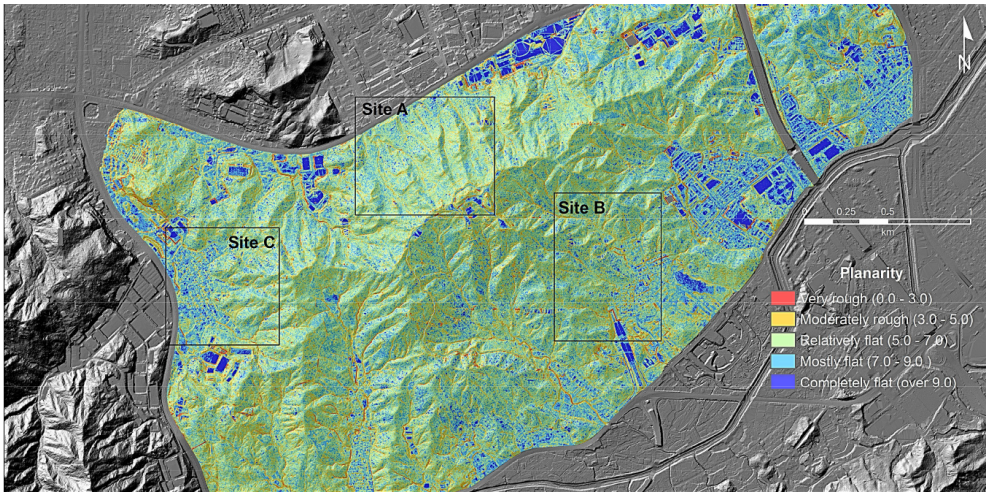

Figure 8. Spatial distribution of the Planarity over the effective study area. Areas outlined in the figure are shown in Figs. 11–13.

NHESSD
2, 7119–7147, 2014

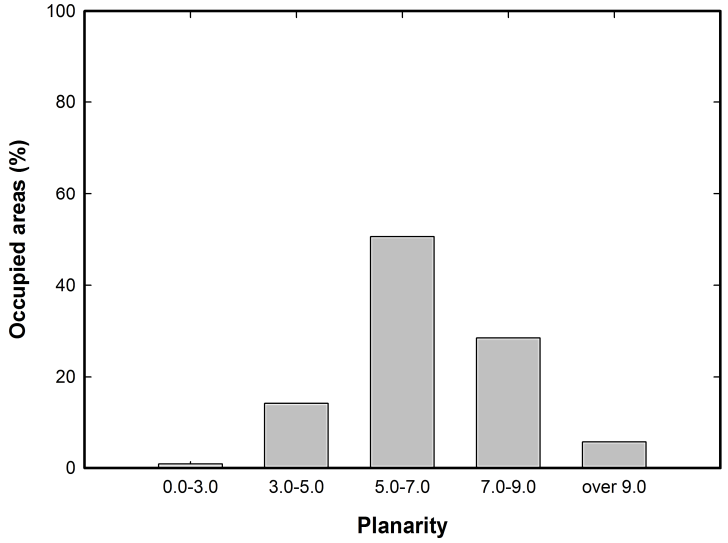

Figure 9. Distribution of representative values of the Planarity over the effective study area.

NHESSD
2, 7119–7147, 2014

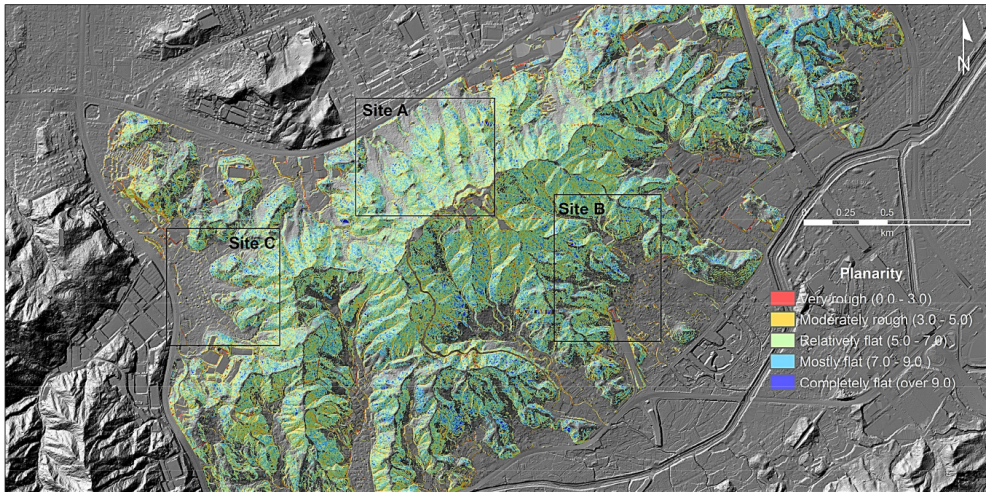

Figure 10. Spatial distribution of the Planarity where the mean slope value of above 19° over the effective study area. Areas outlined in the figure are shown in Figs. 11–13.

NHESSD
2, 7119–7147, 2014

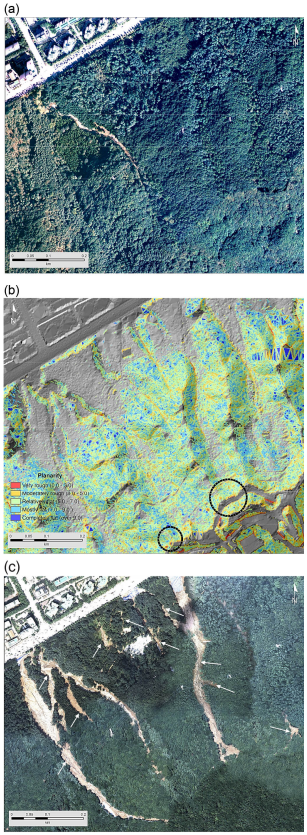

Figure 11. Landslides characteristics in Site A. **(a)** Aerial photograph, before the landslide. **(b)** Modified Planarity. Areas outlined by black circles are supposed to the landslide initiation areas defined by the Planarity of less than three. **(c)** Aerial photograph, after the landslide. White arrows represent observed landslides and their source areas.

NHESSD
2, 7119–7147, 2014

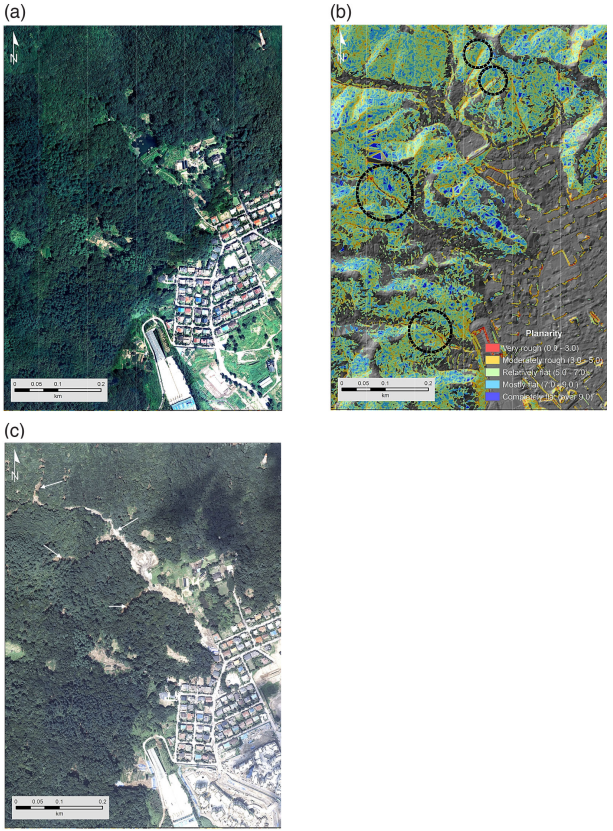

Figure 12. Landslides characteristics in Site B. **(a)** Aerial photograph, before the landslide. **(b)** Modified Planarity. Areas outlined by black circles are supposed to the landslide initiation areas defined by the Planarity of less than three. **(c)** Aerial photograph, after the landslide. White arrows represent observed landslides and their source areas.

NHESSD
2, 7119–7147, 2014

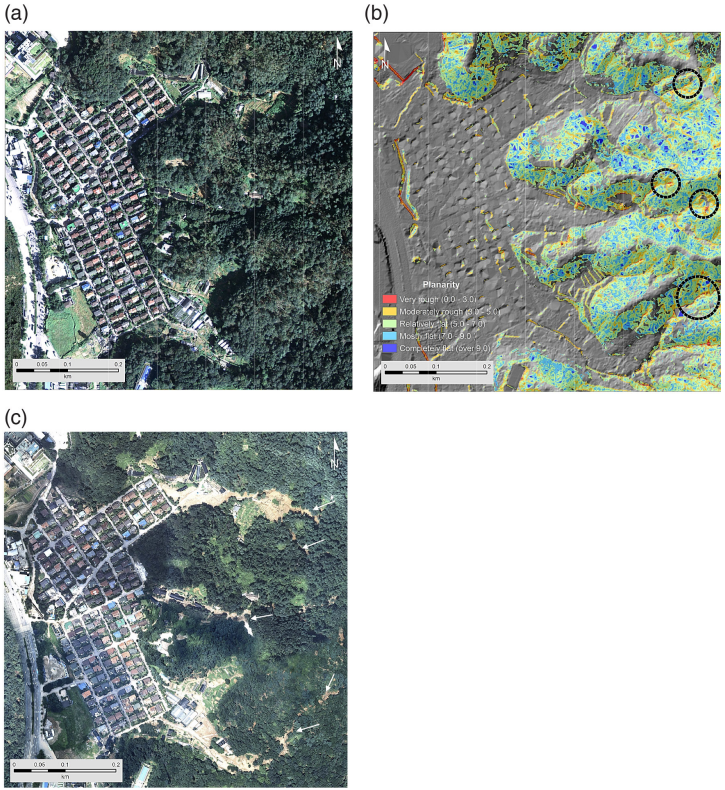

Figure 13. Landslides characteristics in Site C. **(a)** Aerial photograph, before the landslide. **(b)** Modified Planarity. Areas outlined by black circles are supposed to the landslide initiation areas defined by the Planarity of less than three. **(c)** Aerial photograph, after the landslide. White arrows represent observed landslides and their source areas.

NHESSD
2, 7119–7147, 2014